

Quantum energies of BPS vortices in $D = 2 + 1$ and $D = 3 + 1$

N. Graham^{a)}, H. Weigel^{b)}

^{a)}*Department of Physics, Middlebury College Middlebury, VT 05753, USA*

^{b)}*Institute for Theoretical Physics, Physics Department,
Stellenbosch University, Matieland 7602, South Africa*

We consider vortices in scalar electrodynamics and compute the leading quantum correction to their energies for the BPS case of identical classical masses of the Higgs and gauge fields. In particular, we focus on the winding number n dependence of these corrections, from which we can extract the binding energies of configurations with larger n . For both dimensionalities, $D = 2 + 1$ and $D = 3 + 1$, we find that quantum corrections are negative and scale approximately linearly with n , so that combined vortices are favored over isolated ones.

I. INTRODUCTION

The Abrikosov-Nielsen-Olesen (ANO) vortex [1–3] provides the simplest example of a topological soliton with integer winding number, relevant to applications in condensed matter [4], particle physics [5] and cosmology [6, 7]. It arises as a classical solution to the field equations in a theory of scalar electrodynamics with spontaneous symmetry breaking, where the scalar can be the field of Cooper pairs in a superconductor or a Higgs-like field in a particle physics model or a domain wall binding a cosmic string. After spontaneous symmetry breaking, both the scalar and gauge fields have nonzero mass, and for string configurations that are localized in a two-dimensional transverse plane, the magnetic flux through the plane corresponds to a conserved topological winding number. In the Bogomolny-Prasad-Sommerfeld (BPS) [8, 9] case of equal classical masses, which we will focus on here, the classical energy is directly proportional to this flux.

Given this classical field theory picture, it is natural to ask how these results are modified by quantum corrections, and whether the direct proportionality of energy to winding is maintained. To one loop, these corrections consist of the vacuum polarization energy (VPE), the renormalized sum over the zero-point energies $\frac{1}{2}\hbar\omega$ for small oscillations around the classical background. Formally, the VPE is defined as

$$\Delta E = \frac{\hbar}{2} \sum_k \left[\omega_k - \omega_k^{(0)} \right] \Big|_{\text{ren.}}, \quad (1)$$

where ω_k and $\omega_k^{(0)}$ denote the spectra of the quantum fluctuations with and without the vortex background, respectively. The subscript indicates that this divergent sum requires renormalization, which is the primary challenge for the calculation.

Let us briefly explain the renormalization procedure. In the background of a static localized configuration we express the renormalized VPE as the sum

$$\Delta E = E_{\text{b.s.}} + \frac{1}{2} \int_0^\infty dk \sqrt{k^2 + M^2} \left(\Delta\rho(k) - \Delta\rho^{(1)}(k) - \Delta\rho^{(2)}(k) \dots \right) + E_{\text{FD}} + E_{\text{CT}}, \quad (2)$$

where we have chosen natural units with $\hbar = c = 1$. Here $E_{\text{b.s.}}$ is the contribution from the discrete bound states in the potential induced by the background. The contribution from the continuum scattering states is given by the momentum integral, in which the effect of the background is to change the density of states. We call this change $\Delta\rho(k)$. It has a Born expansion in the strength of the potential, and subtracting sufficiently many leading orders of this expansion renders the momentum integral finite. This convergent integral can then be combined with $E_{\text{b.s.}}$ and analytically continued to the imaginary momentum axis. The subtracted Born terms are added back in as Feynman diagrams, E_{FD} , which arise from an equivalent expansion of the effective action. When combined with standard counterterms, E_{CT} , the sum $E_{\text{FD}} + E_{\text{CT}}$ is also finite.

We will use scattering theory to compute the change in the density of states and its Born expansion in a partial wave expansion [10, 11]. Here an additional complication arises as a result of the gauge field winding: scattering theory requires that the background fields vanish at spatial infinity, but string configurations instead approach a nontrivial pure gauge, reflecting the topological winding. To remove this behavior, we use a gauge transformation that makes the fields trivial at infinity, at the cost of introducing a singularity in the gauge field at the origin. The associated magnetic field is unchanged, and remains zero at infinity and finite at the origin. This singularity does not contribute to the final result since it is a gauge artifact, but careful regularization is required to implement it consistently while maintaining gauge symmetry [12].

The first complete treatment of this problem was given in Ref. [13]. There, a more *ad hoc* scheme was used to subtract and add back in terms corresponding to both the renormalization counterterms and the gauge singularity. While in principle the calculations should be equivalent, our approach provides a more systematic separation of the divergences, in the process demonstrating that, surprisingly, a much larger number of partial waves are needed to obtain the large k behavior of $\Delta\rho(k)$ that is consistent with that obtained from analyzing Feynman diagrams. This effect explains some of the discrepancies between our results and previous calculations, some of which appeared to converge without renormalization [14, 15] when too few partial waves are taken into account; including a larger number of partial waves restores the expected divergence. Other discrepancies arise from the peculiarities of the renormalization conditions, which we choose to be on-shell.

In this paper we consider vortices in both $D = 2 + 1$ and $D = 3 + 1$ spacetime dimensions. In the former case, the lower dimension means fewer diagrams are divergent, as is typical in quantum field theory. We nonetheless include finite counterterms to implement the same on-shell renormalization conditions as in $3 + 1$ dimensions, in both cases ensuring that the residues of the propagator poles for both particles, corresponding to the normalization of single-particle states, are left unchanged, as is the pole location for the Higgs particle, corresponding to its mass. The mass of the gauge particle is corrected by quantum effects, so in the end the theory is specified by the two masses, or equivalently by the Higgs mass and the gauge coupling constant. However, while this mass splitting occurs at one-loop order, its effects on the VPE enter at two loops and can be ignored in our calculation. In the case of $3 + 1$ dimensions, the scattering density of states remains the same as in $D = 2 + 1$, but we must use analytic continuation to consistently include the integral over the momentum in the trivial direction [16].

Since the classical BPS vortex has energy proportional to its winding number, the classical energy of a winding n vortex is equal to the energy of n isolated vortices. In the condensed matter system, it represents the boundary between Type I and Type II superconductors. The quantum correction will therefore either stabilize or destabilize the higher winding configurations; by carrying out the calculation through $n = 4$ we find that higher winding is stabilized.

Throughout the paper we treat the $D = 2 + 1$ and $D = 3 + 1$ cases in parallel without introducing separate notations for the most part, and use the context to identify the particular case. In Section II we introduce the classical vortex configuration in singular gauge. The quantization of the theory at one loop and the corresponding on-shell renormalization procedure are described in Sections III and IV, respectively. In Section V we explain the computation of the VPE using scattering data on the imaginary momentum axis and show how we move the divergent contributions from the momentum integral into Feynman diagrams, which are then combined with the counterterms from Section IV. Numerical results are presented and discussed in Section VI, and we give a short summary and conclusion in Section VII. In a short Appendix we estimate the higher-order effects of different masses for the VPE.

II. CLASSICAL SOLUTIONS

We start from the Lagrangian

$$\mathcal{L} = -\frac{1}{4}F_{\mu\nu}F^{\mu\nu} + |D_\mu\Phi|^2 - \frac{\lambda}{4}(|\Phi|^2 - v^2)^2, \quad (3)$$

where as usual $F_{\mu\nu} = \partial_\mu A_\nu - \partial_\nu A_\mu$ and $D_\mu\Phi = (\partial_\mu - ieA_\mu)\Phi$ for an Abelian gauge theory.

In singular gauge, the profiles associated with winding number n are the functions $g(\rho)$ and $h(\rho)$ within the ansätze

$$\Phi_S = vh(\rho) \quad \text{and} \quad \mathbf{A}_S = nv\hat{\varphi}\frac{g(\rho)}{\rho}, \quad (4)$$

where $\rho = evr$ is dimensionless while r is the physical radial coordinate. Here $g(\rho)$ ranges from 0 to 1 and $h(\rho)$ ranges from 1 to 0 as ρ goes from 0 to ∞ .

This field configuration leads to the energy functional

$$E_{\text{cl}} = 2\pi v^2 \int_0^\infty \rho d\rho \left[\frac{n^2}{2} \frac{g'^2}{\rho^2} + h'^2 + n^2 \frac{h^2}{\rho^2} g^2 + \frac{\lambda}{4e^2} (h^2 - 1)^2 \right], \quad (5)$$

where primes denote derivatives with respect to ρ . In $D = 2 + 1$, where v^2 has dimensions of mass, E_{cl} is the vortex energy, while in $D = 3 + 1$, where v has dimensions of mass, it is the energy per unit length of the vortex.

Recalling the tree level mass relations $M_H^2 = \lambda v^2$ and $M_A^2 = 2v^2 e^2$, the coefficient of the last terms becomes

$$\frac{\lambda}{4e^2} = \frac{M_H^2}{2M_A^2},$$

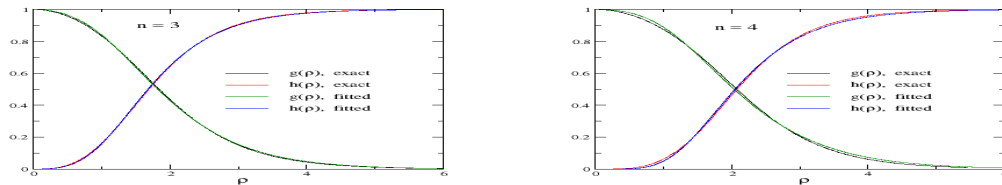


FIG. 1: Comparison of exact and fitted profile functions (from Eq. (9) and Table I) for winding numbers $n = 3$ and $n = 4$.

so that when measured in units of $2\pi v^2$, the classical energy only depends on the ratio of the two masses.

In the BPS case, which we assume henceforth, the coupling constants are related by $\lambda = 2e^2$, *i.e.* $M_H = M_A = M$. Then the energy functional can be written as sums of non-negative quantities plus a surface contribution

$$E_{\text{cl}} = 2\pi v^2 \int_0^\infty \rho d\rho \left\{ \frac{1}{2} \left[\frac{n}{\rho} g' - (h^2 - 1) \right]^2 + \left[h' - \frac{n}{\rho} gh \right]^2 \right\} + 2\pi n v^2 g(h^2 - 1) \Big|_0^\infty. \quad (6)$$

Hence the minimal energy is fully determined by the winding number, yielding $E_{\text{cl}} = 2\pi n v^2 = 2\pi n \frac{M^2}{\lambda}$, with the corresponding profiles obeying the first-order differential equations

$$g' = \frac{\rho}{n}(h^2 - 1) \quad \text{and} \quad h' = \frac{n}{\rho} gh, \quad (7)$$

with the boundary conditions

$$h(0) = 1 - g(0) = 0 \quad \text{and} \quad \lim_{\rho \rightarrow \infty} h(\rho) = 1 - \lim_{\rho \rightarrow \infty} g(\rho) = 1, \quad (8)$$

which correspond to field configurations that approach constant vacuum values at spatial infinity. The topological structure appears through a singularity in the gauge field at the origin, while the magnetic field remains finite everywhere. We have solved the differential equations in (7) numerically, but for later use in the scattering calculation an approximate expression in terms of elementary functions is very helpful. It turns out that for $1 \leq n \leq 4$ the correlation coefficients for the fit

$$h(\rho) = \alpha_2 \tanh^n(\alpha_1 \rho) + [1 - \alpha_2] \tanh^n(\alpha_0 \rho) \quad \text{and} \quad g(\rho) = \beta_1 \rho \frac{1 - \tanh^2(\beta_2 \rho)}{\tanh(\beta_1 \rho)} \quad (9)$$

with the fit parameters α_i and β_i listed in Table I deviate from unity by 10^{-4} or less from the numerical solutions to Eq. (7). The quality of the parameterization is also reflected by the smallness of the relative error $\delta E = E_{\text{fit}}/(2\pi n v^2) - 1$, which is also presented in Tab. I. This accuracy test indicates that the agreement is excellent for $n = 1$ and $n = 2$,

n	α_0	α_1	α_2	β_1	β_2	δE
1	0.8980	0.6621	0.1890	0.5361	0.7689	4.2×10^{-6}
2	0.9072	0.8288	2.6479	1.0949	0.8042	1.9×10^{-5}
3	0.8290	0.7882	5.1953	1.1328	0.7425	1.5×10^{-3}
4	0.7755	0.7350	5.2009	1.1034	0.6853	5.6×10^{-3}

TABLE I: Fit parameters for vortex profiles. The quality of the fit is estimated by the accuracy of the energy: $\delta E = E_{\text{fit}}/(2\pi n v^2) - 1$, where E_{fit} is obtained by substituting (9) into Eq. (5).

but merely good for $n = 3$ and $n = 4$. To show that the fit is nevertheless also suitable in these cases, we display the corresponding profiles in Figure 1. A graphical comparison for $n = 1$ and $n = 2$ does not provide visible differences and we refrain from its presentation.

III. QUANTIZATION

In this Section we quantize the theory, including the relevant ghost fields required for gauge fixing, and derive the equations of motion for the harmonic fluctuations. We will construct the renormalization counterterms in the next Section.

A. Lagrangian for fluctuations

We introduce time-dependent fluctuations about the vortex via

$$\Phi = \Phi_S + \eta \quad \text{and} \quad A^\mu = A_S^\mu + a^\mu \quad (10)$$

and extract the harmonic terms after several integrations by parts as

$$\begin{aligned} \mathcal{L}^{(2)} = & -\frac{1}{2} (\partial_\mu a_\nu) (\partial^\mu a^\nu) + \frac{1}{2} (\partial_\mu a^\mu)^2 + |\Phi_S|^2 a_\mu a^\mu \\ & + |D_\mu \eta|^2 - (|\Phi_S|^2 - 1) |\eta|^2 - \frac{1}{2} (\Phi_S \eta^* + \Phi_S^* \eta)^2 \\ & + i (\Phi_S \eta^* - \Phi_S^* \eta) \partial_\mu a^\mu + 2i a^\mu (\eta^* D_\mu \Phi_S - \eta D_\mu^* \Phi_S^*) a^\mu, \end{aligned} \quad (11)$$

where D_μ is the covariant derivative with the vortex configuration \mathbf{A}_S substituted, $D_0 = \partial_t$ and $\mathbf{D} = \nabla + i n \boldsymbol{\varphi} \frac{g(\rho)}{\rho}$, and we have chosen units with $ev = 1$ such that both particles have classical mass $\sqrt{2}$. The gauge is fixed from the vortex background by adding an R_ξ type Lagrangian with $\xi = 1$ to cancel the $\eta \partial_\mu a^\mu$ term,

$$\mathcal{L}_{\text{gf}} = -\frac{1}{2} [\partial_\mu a^\mu + i (\Phi_S \eta^* - \Phi_S^* \eta)]^2. \quad (12)$$

Collecting the harmonic terms yields

$$\mathcal{L}^{(2)} + \mathcal{L}_{\text{gf}} = -\frac{1}{2} (\partial_\mu a_\nu) (\partial^\mu a^\nu) + |\Phi_S|^2 a_\mu a^\mu + |D_\mu \eta|^2 - (3|\Phi_S|^2 - 1) |\eta|^2 + 2i a^\mu (\eta^* D_\mu \Phi_S - \eta D_\mu^* \Phi_S^*). \quad (13)$$

We still have to subtract the ghost contribution to the VPE associated with the gauge fixing in Eq. (12), which we write as $\mathcal{L}_{\text{gf}} = -\frac{1}{2} G^2$. The infinitesimal gauge transformations reads

$$A^\mu \rightarrow A^\mu + \partial_\mu \chi, \quad \Phi_0 + \eta \rightarrow \Phi_0 + \eta + i\chi(\Phi_0 + \eta) \quad \text{so that} \quad \eta \rightarrow \eta + i\chi(\Phi_0 + \eta). \quad (14)$$

Then

$$\left. \frac{\partial G}{\partial \chi} \right|_{\chi=0} = \partial_\mu \partial^\mu + (2|\Phi_0|^2 + \Phi_0 \eta^* + \Phi_0^* \eta). \quad (15)$$

This induces the ghost Lagrangian (in agreement with Refs. [17, 18])

$$\mathcal{L}_{\text{gh}} = -\partial_\mu \bar{c} \partial^\mu c + 2|\Phi_0| \bar{c} c + \text{non-harmonic terms}. \quad (16)$$

Its VPE is (the negative of) that of a Klein Gordon field of mass $\sqrt{2}$ in the background potential $2(h^2 - 1)$, which can be easily computed. Since it is a complex ghost field, it must be subtracted with a factor of two from the above. Note that from Eq. (13), the non-transverse components of a_μ couple to the same background potential.

In $D = 2 + 1$ the spectrum consists of four real decoupled fields with mass $\sqrt{2}$: $a_1, a_2, \text{Re}(\eta)$ and $\text{Im}(\eta)$. Three other fields, also with mass $\sqrt{2}$, are fully decoupled: a_0 and the two ghosts. The ghosts count negatively, and one of them cancels against the temporal component of the gauge field since they obey the same equation of motion. In total there are then $5 - 2 = 3$ physical degrees of freedom. When computing the VPE, we thus have to subtract a boson type contribution from the background $2(h^2 - 1)$. In $D = 3 + 1$ the gauge field has an additional decoupled longitudinal component, so the non-transverse and ghost contributions cancel completely and we only need to consider a_1 and a_2 together with the complex Higgs field.

B. Wave-equations for quantum fluctuations

To formulate the scattering problem, we employ a partial wave decomposition using the complex combinations

$$a_x + ia_y = \sqrt{2} i e^{-i\omega t} \sum_\ell a_\ell(\rho) e^{i\ell\varphi} \quad \text{and} \quad \eta = e^{-i\omega t} \sum_\ell \eta_\ell(\rho) e^{i\ell\varphi}. \quad (17)$$

We have an analogous expansion for $a_x - ia_y$ and η^* and, in general, a coupled system of four radial functions. In the BPS case, fortunately, this system decouples into two sub-blocks, with the one containing $a_x - ia_y$ and η^* being identical to the above. It will thus suffice to solve

$$\begin{aligned} \frac{1}{\rho} \frac{\partial}{\partial \rho} \rho \frac{\partial}{\partial \rho} \eta_\ell(\rho) &= -q^2 \eta_\ell(\rho) + \left[\frac{\ell^2 - 2n\ell g(\rho) + n^2 g^2(\rho)}{\rho^2} + 3(h^2(\rho) - 1) \right] \eta_\ell(\rho) + \sqrt{2} d(\rho) a_{\ell+1}(\rho) \\ \frac{1}{\rho} \frac{\partial}{\partial \rho} \rho \frac{\partial}{\partial \rho} a_{\ell+1}(\rho) &= -q^2 a_{\ell+1}(\rho) + \left[\frac{(\ell+1)^2}{\rho^2} + 2(h^2(\rho) - 1) \right] a_{\ell+1}(\rho) + \sqrt{2} d(\rho) \eta_\ell(\rho) \end{aligned} \quad (18)$$

with $q^2 = \omega^2 - 2$ and double its VPE. Here the off-diagonal coupling is $d(\rho) = \frac{\partial h(\rho)}{\partial \rho} + \frac{n}{\rho} h(\rho) g(\rho)$.

Finally, the ghost field fully decouples and has a partial wave expansion analogous to the Higgs field in Eq. (17),

$$\frac{1}{\rho} \frac{\partial}{\partial \rho} \rho \frac{\partial}{\partial \rho} \zeta_\ell(\rho) = -q^2 \zeta_\ell(\rho) + \left[\frac{\ell^2}{\rho^2} + 2(h^2(\rho) - 1) \right] \zeta_\ell(\rho). \quad (19)$$

IV. RENORMALIZATION

In this Section we describe the renormalization of the one-loop corrections arising from the fluctuations about the vortex. We begin by analyzing the effective action.

A. Effective actions in $D = 2 + 1$ and $D = 3 + 1$

To identify the ultraviolet divergences in the form of Feynman diagrams [19, 20], we consider the Lagrangian

$$\mathcal{L} = \frac{1}{2} (\partial_\mu \phi) (\partial^\mu \phi^\dagger) - \frac{1}{2} \phi M^2 \phi^\dagger - \phi V \phi^\dagger \quad (20)$$

with four real fields $\phi = (\eta_1, \eta_2, a_x, a_y)$. The Cartesian components of the gauge fields have been defined in Eq. (17) above, while $\eta = (\eta_1 + i\eta_2) / \sqrt{2}$. We then Taylor expand the effective action for these real scalar fields as

$$\begin{aligned} \mathcal{A}_{\text{eff}} &= \frac{i}{2} \text{Tr} \text{Log} [\partial^2 + M^2 - i0^+ + 2V] \\ &= \mathcal{A}_{\text{eff}}^{(0)} + i\text{Tr} [\hat{G}V] - i\text{Tr} [\hat{G}V\hat{G}V] + \frac{4i}{3} \text{Tr} [\hat{G}V\hat{G}V\hat{G}V] - 2i\text{Tr} [\hat{G}V\hat{G}V\hat{G}V\hat{G}V] + \dots, \end{aligned} \quad (21)$$

where $\hat{G} = (\partial^2 + M^2 - i0^+)^{-1}$ times the 4×4 unit matrix. The functional trace is over the space-time coordinates as well as the elements of ϕ and the ellipsis in Eq. (21) represents ultra-violet finite terms. The potential matrix is given by $V = V_0 + V_1 + V_2$, with

$$V_0 = e^2 \begin{pmatrix} \frac{3}{2} (\Phi_S^2 - v^2) & 0 & \sqrt{2} \hat{\mathbf{x}} \cdot \mathbf{A}_S \Phi_S & \sqrt{2} \hat{\mathbf{y}} \cdot \mathbf{A}_S \Phi_S \\ 0 & \frac{3}{2} (\Phi_S^2 - v^2) & -(\sqrt{2}/e) \hat{\mathbf{x}} \cdot \nabla \Phi_S & -(\sqrt{2}/e) \hat{\mathbf{y}} \cdot \nabla \Phi_S \\ \sqrt{2} \hat{\mathbf{x}} \cdot \mathbf{A}_S \Phi_S & -(\sqrt{2}/e) \hat{\mathbf{x}} \cdot \nabla \Phi_S & (\Phi_S^2 - v^2) & 0 \\ \sqrt{2} \hat{\mathbf{y}} \cdot \mathbf{A}_S \Phi_S & -(\sqrt{2}/e) \hat{\mathbf{y}} \cdot \nabla \Phi_S & 0 & (\Phi_S^2 - v^2) \end{pmatrix} \quad (22)$$

and

$$V_1 = e \begin{pmatrix} 0 & 1 & 0 & 0 \\ -1 & 0 & 0 & 0 \\ 0 & 0 & 0 & 0 \\ 0 & 0 & 0 & 0 \end{pmatrix} \mathbf{A}_S \cdot \nabla \quad \text{and} \quad V_2 = \frac{e^2}{2} \begin{pmatrix} 1 & 0 & 0 & 0 \\ 0 & 1 & 0 & 0 \\ 0 & 0 & 0 & 0 \\ 0 & 0 & 0 & 0 \end{pmatrix} \mathbf{A}_S \cdot \mathbf{A}_S \quad (23)$$

Here we have separated out V_1 and V_2 because they relate to the singular terms in the scattering problem, while V_0 is the 4×4 representation of the non-singular terms in Eq. (18). The renormalization program via Feynman diagrams in dimensional regularization is carried out with the full potential matrix V , while the subtractions that we have indicated in Eq. (2) should only involve V_0 supplemented by the wave-function renormalization of the gauge boson, which is simplified by the fake boson trick described below.

B. On-shell renormalization counterterms

The counterterm Lagrangian has four terms,

$$\mathcal{L}_{\text{CT}} = C_g F_{\mu\nu} F^{\mu\nu} + C_h |D_\mu \Phi|^2 + C_0 (\Phi^2 - v^2) + C_V (\Phi^2 - v^2)^2. \quad (24)$$

The C_0 counterterm arises from varying the vacuum expectation value v in the original Lagrangian, Eq. (3). The coefficient is chosen such that it exactly cancels $i\text{Tr} [\hat{G}V_0]$ in Eq. (21), which is the no-tadpole condition. The coefficients C_g and C_h are determined such that the residues of the propagators at the respective masses have no quantum correction, while C_V is fixed such that the pole location of the Higgs propagator (which determines its mass) does not change at one-loop order. The pole location of the gauge field propagator is then an output of the calculation, which can be expressed in terms of the other Lagrangian parameters.

In what follows, D will be the physical dimension while D_ϵ is its continuation in dimensional regularization. That is, for $D = 3 + 1$ we have $D_\epsilon = 4 - 2\epsilon$ and $\epsilon \searrow 0$. We use lower-case letters to denote finite counterterm coefficients; where counterterms diverge, we use the corresponding upper-case letter to denote the coefficients including a divergent part.

To determine the mass and wave-function renormalization we need to expand the effective action to quadratic order in the Higgs and gauge fields. Let us first discuss \mathcal{A}_A , the contributions to the effective action that are quadratic in the gauge field and superficially quadratically divergent, before imposing gauge invariance of the regulator. These contributions arise from the terms linear in V_2 and quadratic in V_1 ,

$$\mathcal{A}_A = C_G \int d^D x F_{\mu\nu} F^{\mu\nu} + i\text{Tr} [\hat{G}V_2] - i\text{Tr} [\hat{G}V_1 \hat{G}V_1], \quad (25)$$

which yields

$$\begin{aligned} \mathcal{A}_A = C_G \int d^D x F_{\mu\nu} F^{\mu\nu} \\ + e^2 \frac{\mu^{3-D_\epsilon}}{(4\pi)^{D_\epsilon/2}} \Gamma\left(1 - \frac{D_\epsilon}{2}\right) \int \frac{d^D k}{(2\pi)^D} \tilde{A}_\mu(k) \tilde{A}^\mu(-k) \int_0^1 dx \left[M^{D_\epsilon-2} - (M^2 - x(1-x)k^2)^{D_\epsilon/2-1} \right], \end{aligned} \quad (26)$$

where $\tilde{A}^\mu(k)$ denotes the Fourier transform of the gauge field. We have repeatedly used $p_\mu \tilde{A}^\mu(k) = 0$, which results from the vortex property $\partial_\mu A^\mu(x) = 0$ and also implies

$$\int d^D x F_{\mu\nu} F^{\mu\nu} = 2 \int \frac{d^D k}{(2\pi)^D} k^2 \tilde{A}_\mu(k) \tilde{A}^\mu(-k). \quad (27)$$

We may also assume $p_\mu \tilde{A}^\mu(k) = 0$ generally when determining the wave-function renormalization C_g because it still allows us to uniquely identify the field strength tensor in the quadratic expansion of the effective action.¹ The residue of the $D = 2$ pole is zero, so the quadratic divergence disappears and we can continue to the dimension of interest. There are additional superficial divergences in $D = 3 + 1$ when expanding the effective action, Eq. (21). However, the logarithmic divergences from $V_0 \otimes V_2$ and $V_0 \otimes V_1 \otimes V_1$ cancel, as do those from $V_2 \otimes V_2$, $V_2 \otimes V_1 \otimes V_1$ and $V_1 \otimes V_1 \otimes V_1 \otimes V_1$. Hence the quadratic order in V is sufficient to implement renormalization.

To collect all terms that are quadratic in the fields we introduce $\tilde{v}_H(k)$ and $\tilde{a}(k)$ as the Fourier transforms of

$$v_H = \Phi_S^2 - v^2 \quad \text{and} \quad a = \sqrt{2}e \begin{pmatrix} e\hat{x} \cdot \mathbf{A}_S \Phi_S & e\hat{y} \cdot \mathbf{A}_S \Phi_S \\ -\hat{x} \cdot \nabla \Phi_S & -\hat{y} \cdot \nabla \Phi_S \end{pmatrix}, \quad (28)$$

respectively. For example, $\tilde{v}_H(k) = \int d^4 x [\Phi_S^2 - v^2] e^{ik_\mu x^\mu}$. In $D = 2 + 1$ we then have

$$\begin{aligned} \mathcal{A}^{(3)} = \int d^3 x \left[c_g F_{\mu\nu} F^{\mu\nu} + c_h (D_\mu \Phi)^* (D^\mu \Phi) + c_v (\Phi \Phi^* - v^2)^2 \right] \\ + \frac{1}{8\pi M} \int \frac{d^3 k}{(2\pi)^3} \left[\frac{11e^4}{2} \tilde{v}_H(k) \tilde{v}_H(-k) + 2\text{tr} (\tilde{a}(k) \tilde{a}^\dagger(-k)) \right] \int_0^1 \frac{dx}{\sqrt{1-x(1-x)k^2/M^2}} \\ - \frac{e^2 M}{4\pi} \int \frac{d^3 k}{(2\pi)^3} \tilde{F}_{\mu\nu}(k) \tilde{F}^{\mu\nu}(-k) \frac{1}{k^2} \int_0^1 dx \left[1 - \sqrt{1-x(1-x)k^2/M^2} \right] + \dots, \end{aligned} \quad (29)$$

¹ If there was parity violation, the dual field strength tensor would also contribute and the assumption would not be justified.

where the ellipsis refer to terms of cubic and higher order. In $D = 3 + 1$ these contributions have divergences, so we write

$$c_g = C_g - \frac{e^2}{192\pi^2} (C_\epsilon + 1), \quad c_h = C_h - \frac{e^2}{4\pi^2} C_\epsilon, \quad c_v = C_V + \frac{13e^4}{32\pi^2} C_\epsilon, \quad (30)$$

with $C_\epsilon = \frac{1}{\epsilon} - \gamma + \ln\left(4\pi\frac{\Lambda^2}{M^2}\right)$ from dimensional regularization with scale Λ . The second-order effective action is then

$$\begin{aligned} \mathcal{A}^{(4)} = & \int d^4x \left[c_g F_{\mu\nu} F^{\mu\nu} + c_h (D_\mu \Phi)^* (D^\mu \Phi) + c_v (\Phi \Phi^* - v^2)^2 \right] \\ & - \frac{1}{8\pi^2} \int \frac{d^4k}{(2\pi)^4} \left[\frac{13e^4}{4} \tilde{v}_H(k) \tilde{v}_H(-k) + \text{tr}(\tilde{a}(k) \tilde{a}^\dagger(-k)) \right] \int_0^1 dx \ln [1 - x(1-x)k^2/M^2] \\ & - \frac{1}{2} \left(\frac{eM}{4\pi} \right)^2 \int \frac{d^4k}{(2\pi)^4} \tilde{F}_{\mu\nu}(k) \tilde{F}^{\mu\nu}(-k) \frac{1}{k^2} \int_0^1 dx [1 - x(1-x)k^2/M^2] \ln [1 - x(1-x)k^2/M^2] + \dots \end{aligned} \quad (31)$$

Here all counterterm coefficients are finite and thus written in lower case. Comparing the $D = 2 + 1$ and $D = 3 + 1$ cases, a change in the relative coefficients between the $\tilde{v}_H(k) \tilde{v}_H(-k)$ and $\tilde{a}(k) \tilde{a}^\dagger(-k)$ is observed. This change results from the ghost contribution in $D = 2 + 1$.

Next, we write the part of the action which is quadratic in the fields (including the tree level counterterms) as

$$\mathcal{A}^{(D)} = \int \frac{d^D k}{(2\pi)^D} \left[G_H^{(D)} \tilde{h}(k) \tilde{h}(-k) + G_A^{(D)} \tilde{A}_\mu(k) \tilde{A}^\mu(-k) \right], \quad (32)$$

where $\tilde{h}(k)$ is the Fourier transform of $h(x) = \Phi(x) - v$. In general (but not for the vortex) there are also terms like $\tilde{h}(k) k_\mu \tilde{A}^\mu(-k)$, but they need not to be considered for our renormalization conditions, because they would determine the renormalized coupling. For the Higgs part we find, using $M = \sqrt{2}ev$,

$$\begin{aligned} G_H^{(3)}(k^2) &= \left(\frac{1}{2} + c_h \right) k^2 - \left(\frac{M^2}{2} - 4v^2 c_v \right) + \frac{e^2}{8\pi M} (11M^2 - 4k^2) \int_0^1 \frac{dx}{\sqrt{1 - x(1-x)k^2/M^2}} \\ G_H^{(4)}(k^2) &= \left(\frac{1}{2} + c_h \right) k^2 - \left(\frac{M^2}{2} - 4v^2 c_v \right) - \frac{e^2}{16\pi^2} (13M^2 - 4k^2) \int_0^1 dx \ln [1 - x(1-x)k^2/M^2]. \end{aligned} \quad (33)$$

The gauge part is obtained from setting $\Phi = v$,

$$\begin{aligned} G_A^{(3)}(k^2) &= -\frac{1}{2} (1 - 4c_g) k^2 + (1 + c_h) \frac{M^2}{2} - \frac{e^2 M}{4\pi} \int_0^1 \frac{dx}{\sqrt{1 - x(1-x)k^2/M^2}} \\ &\quad - \frac{e^2 M}{2\pi} \int_0^1 dx \left[1 - \sqrt{1 - x(1-x)k^2/M^2} \right] \\ G_A^{(4)}(k^2) &= -\frac{1}{2} (1 - 4c_g) k^2 + (1 + c_h) \frac{M^2}{2} + 2 \left(\frac{eM}{4\pi} \right)^2 \int_0^1 dx \ln [1 - x(1-x)k^2/M^2] \\ &\quad - \left(\frac{eM}{4\pi} \right)^2 \int_0^1 dx [1 - x(1-x)k^2/M^2] \ln [1 - x(1-x)k^2/M^2] \end{aligned} \quad (34)$$

The on-shell renormalization conditions for the Higgs field are

$$G_H^{(D)}(M^2) = 0 \quad \text{and} \quad \left. \frac{\partial G_H^{(D)}(k^2)}{\partial k^2} \right|_{k^2=M^2} = \frac{1}{2}. \quad (35)$$

from which we obtain for $D = 2 + 1$

$$c_h = \frac{e^2}{48\pi M} [45 \ln(3) - 28] \quad \text{and} \quad c_v = \frac{e^4}{96\pi M} [28 - 87 \ln(3)], \quad (36)$$

and for $D = 3 + 1$ we find

$$c_h = \frac{e^2}{16\pi^2} \left[17 - \frac{10\pi}{\sqrt{3}} \right] \quad \text{and} \quad c_v = \frac{e^4}{32\pi^2} \left[19 \frac{\pi}{\sqrt{3}} - 35 \right]. \quad (37)$$

The gauge field renormalization conditions are

$$G_A^{(D)}(M_A^2) = 0 \quad \text{and} \quad \left. \frac{\partial G_A^{(D)}(k^2)}{\partial k^2} \right|_{k^2=M_A^2} = -\frac{1}{2}. \quad (38)$$

From this we determine the unknowns c_g and M_A , where the latter is written in terms of the ratio $\mu = \frac{M_A}{M}$. We obtain for $D = 2 + 1$

$$c_g(\mu) = \frac{e^2}{32\pi M} \left[\frac{2}{4 - \mu^2} + \frac{1}{\mu} \operatorname{atanh} \left(\frac{\mu}{2} \right) \right] \quad (39)$$

and for $D = 3 + 1$

$$c_g(\mu) = -\frac{e^2}{288\pi^2} \frac{1}{\mu^3} \left[\mu(\mu^2 - 12) \mu + 3 \frac{\mu^4 - 2\mu^2 + 16}{\sqrt{4 - \mu^2}} \operatorname{asin} \left(\frac{\mu}{2} \right) \right]. \quad (40)$$

Within the one-loop order $c_i = \mathcal{O}(\hbar)$ and $\mu^2 - 1 = \mathcal{O}(\hbar)$ so that $c_g(\mu) - c_g(1) = \mathcal{O}(\hbar^2)$.

Finally, we combine these results to compute the mass ratio μ in terms of the Lagrangian parameter e . We obtain for $D = 2 + 1$

$$\frac{2\pi M}{e^2} (\mu^2 - 1) = \frac{15}{8} \ln(3) - \frac{7}{6} + \frac{\mu^2}{2(4 - \mu^2)} - 1 - \frac{\mu}{4} \operatorname{atanh} \left(\frac{\mu}{2} \right) \quad (41)$$

and $D = 3 + 1$

$$\frac{8\pi^2}{e^2} (\mu^2 - 1) = \frac{9}{2} - \frac{5\pi}{\sqrt{3}} - \frac{\mu^2}{6} + \frac{16 - 2\mu^2}{\mu\sqrt{4 - \mu^2}} \operatorname{asin} \left(\frac{\mu}{2} \right). \quad (42)$$

At one-loop order to the VPE it is fully consistent to use $\mu = 1$ in the finite parts of the counterterm coefficients. Nevertheless, in Appendix A we will briefly discuss effects resulting from $c_g(\mu) - c_g(1) \neq 0$.

C. Fake boson subtraction

As seen from Eq. (2), the computation of the VPE requires us to move divergent terms from the non-perturbative contribution (which is obtained from scattering data) to Feynman diagrams. For the remaining logarithmic divergence in Eq. (26) with $D = 3 + 1$, this is not possible for the vortex configuration since neither its Fourier transform nor its Born approximation to the scattering data exist. We instead introduce the fake boson technique, in which we begin by considering bosonic fluctuations about the static potential $V(x) = V_f(r)$. We take this boson field to be complex because its scattering data will later be combined with those from the complex vortex fluctuations in Eq. (18). The second-order effective action for this boson field is

$$\begin{aligned} \mathcal{A}_{(\text{fb})} &= \frac{1}{2(4\pi)^2} \left[\frac{1}{\epsilon} - \gamma + \ln \left(\frac{4\pi\mu^2}{M^2} \right) \right] \int d^4x V_f^2 \\ &\quad - \frac{1}{2(4\pi)^2} \int \frac{d^4k}{(2\pi)^4} \tilde{V}_f(k) \tilde{V}_f(-k) \int_0^1 dx \ln \left[1 - x(1-x) \frac{k^2}{M^2} \right], \end{aligned} \quad (43)$$

with the Fourier transform $\tilde{V}(k) = \int d^Dx V(x) e^{ik_\nu x^\nu}$. We define the normalization of $V_f(r)$ such that the $1/\epsilon$ in singularities in Eq. (43) match those of C_g . That is, for the given potential V_f we scale all second order contributions by the factor c_B , which is determined from

$$-\frac{6c_B}{e^2} \int \frac{d^4x}{TL} V_f^2 = \int \frac{d^4x}{TL} F_{\mu\nu} F^{\mu\nu} = 4\pi v^2 \int_0^\infty \rho d\rho \left(\frac{n^2 g'^2}{\rho} \right)^2, \quad (44)$$

where TL is the volume of the subspace in which the vortex is translationally invariant. Then we end up with the finite expression

$$\begin{aligned} C_g \int \frac{d^4x}{TL} F_{\mu\nu} F^{\mu\nu} + c_B \mathcal{A}_2^{(\text{fb})} &= \frac{M^2}{288\pi} [22 - 5\sqrt{3}\pi] \int_0^\infty \rho d\rho \left(n \frac{g'}{\rho} \right)^2 \\ &\quad + c_B \frac{M^2}{16\pi} \int_0^\infty dq \tilde{v}_f^2(q) \left[\sqrt{q^2 + 8} \operatorname{asinh} \left(\frac{q}{\sqrt{8}} \right) - q \right], \end{aligned} \quad (45)$$

where $\tilde{v}_f(q) = \int_0^\infty \rho d\rho V_f(r) J_0(q\rho)$ and J_0 is a cylindrical Bessel function.

Above we have outlined the fake boson approach for $D = 3 + 1$, where it is needed to remove an ultra-violet divergence. Though it is not required in $D = 2 + 1$, we apply it there as well because the numerical evaluation of the momentum space integrals in Sec. V is more stable with the corresponding subtraction. The correspondingly renormalized part of the action is

$$C_g \int d^3x F_{\mu\nu} F^{\mu\nu} + c_B \mathcal{A}_2^{(\text{fb})} = -\frac{M}{96} [4 + 3 \ln(3)] \int_0^\infty \rho d\rho \left(n \frac{g'}{\rho} \right)^2 - c_B \frac{M}{4\sqrt{2}} \int_0^\infty dq \tilde{v}_f^2(q) \arctan \left(\frac{q}{\sqrt{8}} \right). \quad (46)$$

V. VACUUM POLARIZATION ENERGY (VPE)

With all the ingredients of the calculation determined, we next show how to assemble them to determine the fully renormalized VPE.

A. Relevance of scattering data

In this Section we briefly review the spectral methods for computing the VPE of static, extended field configurations from Ref. [11].

The background field configuration induces a potential for small amplitude fluctuations, which are treated by standard techniques of scattering theory in quantum mechanics. These calculations provide the bound state energies, ω_j , which directly enter the VPE, as well as the phase shifts $\delta(k)$, or more generally the scattering matrix, as functions of the wave-number k for single-particle energies above the threshold given by the mass m of the fluctuating field. Those phase shifts parameterize the change in the density of continuum modes via the Friedel-Krein formula [21],

$$\Delta\rho_\ell = \frac{1}{\pi} \frac{d\delta_\ell(k)}{dk}, \quad (47)$$

where ℓ indexes the partial wave-expansion in Eq. (17). As shown in Eq. (2), that change determines the continuum contribution to the VPE

$$\Delta E = \frac{1}{2} \sum_j^{\text{b.s.}} \omega_j + \int_0^\infty \frac{dk}{2\pi} \sum_\ell \sqrt{k^2 + m^2} \frac{d\delta_\ell(k)}{dk} + E_{\text{CT}}. \quad (48)$$

Our scattering problem is in two space dimensions and all angular momentum sums run over the integers from negative to positive infinity.

Next we describe how the counterterms cancel the divergences originating from the large k behavior of the phase shift in the momentum integral. In the previous Section we have shown that the Feynman diagrams are generated by expanding the effective action in powers of the potential appearing in the scattering wave-equations. The equivalent Born expansion for the phase shifts is most efficiently performed within the variable phase approach [22], which factors out the outgoing wave from the full wave-function. We will provide details of that approach for the vortex problem in the next Section and restrict ourselves here to the description of the main concepts. The factor function is called the Jost solution $\mathcal{F}_\ell(r, k)$, and the differential equation for the Jost solution is (numerically) solved with the boundary condition $\lim_{r \rightarrow \infty} \mathcal{F}(r, k) = \mathbf{1}$. In a multi-channel problem $\mathcal{F}_\ell(r)$ is matrix-valued. Regularity of the scattering wave-function then determines the scattering matrix and subsequently the phase shift for a particular partial wave

$$\delta_\ell(k) = \frac{1}{2i} \ln \det \lim_{r \rightarrow 0} [\mathcal{F}_\ell^*(r, k) \mathcal{F}_\ell^{-1}(r, k)].$$

Most importantly, the Jost solution has a perturbation expansion in powers of the scattering potential: $\mathcal{F}_\ell(r, k) = \mathbf{1} + \mathcal{F}_\ell^{(1)}(r, k) + \mathcal{F}_\ell^{(2)}(r, k) + \dots$ with boundary conditions $\lim_{r \rightarrow \infty} \mathcal{F}_\ell^{(n)}(r, k) = 0$. The individual contributions can be straightforwardly obtained by iterating the wave-equation. This expansion in turn induces the Born series for the phase shift,

$$\begin{aligned} \delta_\ell^{(1)}(k) &= \frac{1}{2i} \lim_{r \rightarrow 0} \text{tr} \left[\mathcal{F}_\ell^{(1)*}(r, k) - \mathcal{F}_\ell^{(1)}(r, k) \right], \\ \delta_\ell^{(2)}(k) &= \frac{1}{2i} \lim_{r \rightarrow 0} \text{tr} \left[\mathcal{F}_\ell^{(2)*}(r, k) - \mathcal{F}_\ell^{(2)}(r, k) - \frac{1}{2} [\mathcal{F}_\ell^{(1)}(r, k)]^2 + \frac{1}{2} [\mathcal{F}_\ell^{(1)*}(r, k)]^2 \right], \quad \text{etc.} \end{aligned} \quad (49)$$

Since the phase shift is dimensionless, the expansion in powers of the potential is also an expansion in the inverse momentum. Hence taking sufficiently many terms, N , from the Born series and subtracting them from the phase shift will render the momentum integral in Eq. (48) finite. We then add these subtractions back via the equivalent Feynman expansion up to order N that we developed in the previous Section,

$$\Delta E = \frac{1}{2} \sum_j^{\text{b.s.}} \omega_j + \int_0^\infty \frac{dk}{2\pi} \sum_\ell \sqrt{k^2 + m^2} \frac{d}{dk} \left[\delta_\ell(k) - \delta_\ell^{(1)}(k) - \delta_\ell^{(2)}(k) - \dots - \delta_\ell^{(N)}(k) \right] + E_{\text{FD}}^{(N)} + E_{\text{CT}}. \quad (50)$$

The sum $E_{\text{FD}}^{(N)} + E_{\text{CT}}$ combines to form an ultra-violet finite expression as, for example, for the action in Eqs. (29) and (31). We note that this process is exact within one loop and does not rely on the accuracy of the Born approximation.

To further process the momentum integral we recall that the Jost function² $\mathcal{F}(k) = \lim_{r \rightarrow 0} \mathcal{F}(r, k)$ is analytic for $\text{Im}(k) \geq 0$ and that for real k its complex conjugate is $\mathcal{F}^*(k) = \mathcal{F}(-k)$ [23]. Thus we write $\delta_\ell(k) = (1/2i) [\ln \det \mathcal{F}_\ell(-k) - \ln \det \mathcal{F}_\ell(k)]$ and extend the integral over the full real axis. With the Born subtractions made above, there will be no contribution to the integral from a semi-circle at infinitely large $|k|$ for $\text{Im}(k) \geq 0$, and we may thus close the contour accordingly. However, we have to circumvent the branch cut that emerges in $\sqrt{k^2 + m^2}$ for $\text{Im}(k) > m$. That will leave a contribution along the imaginary k axis starting at im that picks up the discontinuity of the square root. Finally, we collect the residues that emerge from the zeros of the Jost function, which create first-order poles in the logarithmic derivative. These zeros are known to be single and located at the wave-numbers corresponding to the bound state energies: $k_j = i\sqrt{m^2 - \omega_j^2}$ [23]. By virtue of Cauchy's theorem, these residues exactly cancel the discrete bound state contribution in the VPE [24]. Introducing $t = k/i$ and $\nu_\ell(t) = \ln \det \mathcal{F}_\ell(it)$ and integrating by parts, we obtain the compact expression

$$\Delta E = \int_m^\infty \frac{dt}{2\pi} \frac{t}{\sqrt{t^2 - m^2}} \sum_\ell \left[\nu_\ell(t) - \nu_\ell^{(1)}(t) - \nu_\ell^{(2)}(t) - \dots - \nu_\ell^{(N)}(t) \right] + E_{\text{FD}}^{(N)} + E_{\text{CT}}, \quad (51)$$

where the $\nu_\ell^{(n)}(t)$ arise from the Born series expansion of $\mathcal{F}_\ell(it)$.

The situation in $D = 3+1$ is slightly more complicated. The vortex is translationally invariant along the symmetry axis (which we choose to be in the z direction). The wave-function has a plane wave factor for the dependence of that coordinate and we have to integrate over the corresponding momentum. Since the phase shifts do not depend on that momentum, there is no Born subtraction that removes the ultra-violet divergence emerging from that integration. The solution is the so-called interface formalism developed in Ref. [16], in which that integral is dimensionally regularized in $d - 1$ space dimensions, showing that the divergence is proportional to

$$\frac{1}{d-1} \left\{ \int_0^\infty \frac{dk}{\pi} k^2 \frac{d}{dk} \sum_\ell \left[\delta_\ell(k) - \delta_\ell^{(1)}(k) - \delta_\ell^{(2)}(k) - \dots - \delta_\ell^{(N)}(k) \right] + \sum_j^{\text{b.s.}} \omega_j^2 - m^2 \right\}.$$

The expression in curly brackets actually vanishes in all partial wave channels individually via one of the sum rules that generalize Levinson's theorem [25], which follow from analyticity of the Jost function for $\text{Im}(k) \geq 0$. Thus the limit $d \rightarrow 1$ can be taken, yielding

$$\Delta E = \frac{-1}{8\pi} \left[\int_0^\infty \frac{dk}{\pi} \sum_\ell \omega^2(k) \ln \frac{\omega^2(k)}{\bar{\Lambda}^2} \frac{d}{dk} \left[\nu_\ell(t) - \nu_\ell^{(1)}(t) - \nu_\ell^{(2)}(t) - \dots - \nu_\ell^{(N)}(t) \right] + \sum_j^{\text{b.s.}} \omega_j^2 \ln \frac{\omega_j^2}{\bar{\Lambda}^2} \right] + E_{\text{FD}}^{(N)} + E_{\text{CT}} \quad (52)$$

as the VPE per unit length of the vortex. The arbitrary energy scale $\bar{\Lambda}$ has been introduced for dimensional reasons. It cancels in Eq. (52) by a generalization of Levinson's theorem. Again, by closing the contour in the upper half k -plane, we can remove the explicit bound state contribution. This time we pick up the discontinuity from the logarithm,

$$\Delta E = \int_m^\infty \frac{dt}{4\pi} t \sum_\ell \left[\nu_\ell(t) - \nu_\ell^{(1)}(t) - \nu_\ell^{(2)}(t) - \dots - \nu_\ell^{(N)}(t) \right] + E_{\text{FD}}^{(N)} + E_{\text{CT}}. \quad (53)$$

² The general definition of the Jost function is the Wronskian of the Jost and regular solutions.

B. Jost function for scattering about the vortex

Because the singularity of the vortex field configuration at its center makes it impossible to straightforwardly apply the standard form of the spectral methods described above. In this Section we explain the required modifications. As described above, the ultra-violet singularities that occur at third and higher order in the expansion of the effective action cancel (when regularized in a gauge invariant scheme), so we may set $N = 2$ hereafter.

We return to the dimensionless variables $\rho = evr$ and $q = k/ev$ that enter the wave-equations (18). We define the Jost solution by introducing $\Psi_\ell \sim \begin{pmatrix} \eta_\ell \\ a_{\ell+1} \end{pmatrix}$ in scattering channel ℓ as a 2×2 matrix with the free solution factored out,

$$\Psi_\ell = \mathcal{F}_\ell \cdot \mathcal{H}_\ell \quad \text{where} \quad \mathcal{H}_\ell = \begin{pmatrix} H_\ell^{(1)}(q\rho) & 0 \\ 0 & H_{\ell+1}^{(1)}(q\rho) \end{pmatrix}, \quad (54)$$

with boundary condition $\lim_{\rho \rightarrow \infty} \mathcal{F}_\ell = \mathbf{1}$. Since the two columns of \mathcal{H}_ℓ represent free outgoing cylindrical waves for either η_ℓ or $a_{\ell+1}$, the physical scattering solution is

$$\Psi_\ell^{\text{sc}} = \mathcal{F}_\ell^* \cdot \mathcal{H}_\ell^* - \mathcal{F}_\ell \cdot \mathcal{H}_\ell \cdot \mathcal{S}_\ell,$$

where \mathcal{S}_ℓ is the scattering matrix, which can be extracted using $\lim_{\rho \rightarrow 0} \Psi_{\text{sc}} = 0$. Then $\mathcal{F}_\ell = \mathcal{F}_\ell(\rho, q)$ is the Jost solution, which leads to the Jost function $\mathcal{F}_\ell(q) = \lim_{\rho \rightarrow 0} \mathcal{F}_\ell(\rho, q)$. In both cases, $D = 2 + 1$ and $D = 3 + 1$, a major ingredient for the scattering piece of the VPE is the Jost function for imaginary momenta $\nu_\ell(t) = \ln \det [\mathcal{F}_\ell(it)]$. In matrix form, the scattering differential equations read

$$\frac{\partial^2}{\partial \rho^2} \mathcal{F}_\ell = -\frac{\partial}{\partial \rho} \mathcal{F}_\ell - 2 \left(\frac{\partial}{\partial \rho} \mathcal{F}_\ell \right) \cdot \mathcal{Z}_\ell + \frac{1}{\rho^2} [\mathcal{L}_\ell, \mathcal{F}_\ell] + \mathcal{V}_\ell \cdot \mathcal{F}_\ell. \quad (55)$$

The angular momenta enter via the derivative matrix for the analytically continued Bessel functions

$$\mathcal{Z}_\ell = \begin{pmatrix} \frac{|\ell|}{\rho} - t \frac{K_{|\ell+1}(t\rho)}{K_{|\ell}(t\rho)} & 0 \\ 0 & \frac{|\ell+1|}{\rho} - t \frac{K_{|\ell+1+1}(t\rho)}{K_{|\ell+1}(t\rho)} \end{pmatrix} \quad \text{and} \quad \mathcal{L}_\ell = \begin{pmatrix} \ell^2 & 0 \\ 0 & (\ell+1)^2 \end{pmatrix}, \quad (56)$$

and the potential matrix is

$$\mathcal{V}_\ell = \begin{pmatrix} 3(h^2(\rho) - 1) + \frac{1}{\rho^2}(n^2 g^2(\rho) - 2n\ell g(\rho)) & \sqrt{2}d(\rho) \\ \sqrt{2}d(\rho) & 2(h^2(\rho) - 1) \end{pmatrix}. \quad (57)$$

The standard procedure to determine the Born approximations, which are needed to regularize the ultraviolet divergences, fails when $g(0) \neq 0$ [26]. This can be seen by noting that the integral $\int_0^\infty \rho d\rho \left(\frac{g(\rho)}{\rho} \right)^2$, which would appear in the leading Born approximation for the gauge field potential, is ill-defined in the singular gauge. To perform the Born subtractions without the singular terms, we introduce

$$\bar{\mathcal{V}} = \begin{pmatrix} 3(h^2(\rho) - 1) & \sqrt{2}d(\rho) \\ \sqrt{2}d(\rho) & 2(h^2(\rho) - 1) \end{pmatrix} \quad (58)$$

and iterate the auxiliary differential equation

$$\frac{\partial^2}{\partial \rho^2} \bar{\mathcal{F}}_\ell = -\frac{\partial}{\partial \rho} \bar{\mathcal{F}}_\ell - 2 \left(\frac{\partial}{\partial \rho} \bar{\mathcal{F}}_\ell \right) \cdot \mathcal{Z}_\ell + \frac{1}{\rho^2} [\mathcal{L}_\ell, \bar{\mathcal{F}}_\ell] + \bar{\mathcal{V}} \cdot \bar{\mathcal{F}}_\ell \quad (59)$$

according to the expansion $\bar{\mathcal{F}}_\ell = \mathbf{1} + \bar{\mathcal{F}}_\ell^{(1)} + \bar{\mathcal{F}}_\ell^{(2)} + \dots$. The relevant leading orders are

$$\begin{aligned} \frac{\partial^2}{\partial \rho^2} \bar{\mathcal{F}}_\ell^{(1)} &= -\frac{\partial}{\partial \rho} \bar{\mathcal{F}}_\ell^{(1)} - 2 \left(\frac{\partial}{\partial \rho} \bar{\mathcal{F}}_\ell^{(1)} \right) \cdot \mathcal{Z}_\ell + \frac{1}{\rho^2} [\mathcal{L}_\ell, \bar{\mathcal{F}}_\ell^{(1)}] + \bar{\mathcal{V}}, \\ \frac{\partial^2}{\partial \rho^2} \bar{\mathcal{F}}_\ell^{(2)} &= -\frac{\partial}{\partial \rho} \bar{\mathcal{F}}_\ell^{(2)} - 2 \left(\frac{\partial}{\partial \rho} \bar{\mathcal{F}}_\ell^{(2)} \right) \cdot \mathcal{Z}_\ell + \frac{1}{\rho^2} [\mathcal{L}_\ell, \bar{\mathcal{F}}_\ell^{(2)}] + \bar{\mathcal{V}} \cdot \bar{\mathcal{F}}_\ell^{(1)}, \end{aligned} \quad (60)$$

and all $\bar{\mathcal{F}}_\ell^{(m)}$ vanish in the limit $\rho \rightarrow \infty$. From the differential equations (55) and (60) we extract

$$\nu_\ell(t) = \lim_{\rho \rightarrow \rho_{\min}} \ln \det \mathcal{F}_\ell, \quad \bar{\nu}_\ell^{(1)}(t) = \lim_{\rho \rightarrow \rho_{\min}} \text{tr} \bar{\mathcal{F}}_\ell^{(1)} \quad \text{and} \quad \bar{\nu}_\ell^{(2)}(t) = \lim_{\rho \rightarrow \rho_{\min}} \text{tr} \left[\bar{\mathcal{F}}_\ell^{(2)} - \frac{1}{2} \left(\bar{\mathcal{F}}_\ell^{(1)} \right)^2 \right] \quad (61)$$

where ρ_{\min} is a tiny but nonzero number. The above expansion is the analog of Eq. (49) for the Jost function of the vortex with imaginary momentum, but our Born subtraction no longer includes the singular terms; we describe how to handle them below.

The Jost functions for the ghost and fake boson are analogous to the above, but much simpler. The Jost solution is no longer a matrix, so the commutator term disappears. Then one just replaces \mathcal{V} and $\bar{\mathcal{V}}$ by $2v^2 [h^2(\rho) - 1]$ for the ghost and by $V_f(\rho)$ for the fake boson. Furthermore, the angular momentum sum is symmetric in $\ell \rightarrow -\ell$, so it can be simplified to run over non-negative values with a degeneracy factor of two for $\ell \geq 1$.

By subtracting just $\bar{\nu}_\ell^{(1)}(t)$ and $\bar{\nu}_\ell^{(2)}(t)$ from $\nu_\ell(t)$ we do not include the subtractions for the singular terms that, in a gauge-invariant formulation, induce a logarithmic ultra-violet divergence for $D = 3 + 1$. To investigate the relevant diagrams we compare the dimensional and sharp cut-off regularization schemes, leading to the identification (with an arbitrary mass scale Λ),

$$\frac{1}{\epsilon(4\pi)^2} = -i \int \frac{d^4 l}{(2\pi)^4} \frac{1}{(l^2 - \Lambda^2 + i0^+)^2} \Big|_{\text{div.}} = \frac{1}{8\pi^2} \int \frac{l^2 dl}{\sqrt{l^2 + \Lambda^2}^3} \Big|_{\text{div.}}, \quad (62)$$

We thus expect for $\rho_{\min} \rightarrow 0$

$$[\nu(t)]_V := \lim_{L \rightarrow \infty} \sum_{\ell=-L}^L \left[\nu_\ell(t) - \bar{\nu}_\ell^{(1)}(t) - \bar{\nu}_\ell^{(2)}(t) \right]_{\rho_{\min}} - n^2 \int_{\rho_{\min}}^{\infty} \frac{d\rho}{\rho} g^2(\rho) \xrightarrow{t \rightarrow \infty} \frac{n^2}{12t^2} \int_0^{\infty} \frac{d\rho}{\rho} \left(\frac{dg(\rho)}{d\rho} \right)^2. \quad (63)$$

Again, the superscripts denote the Born expansion order with respect to $\bar{\mathcal{V}}$. As explained in Ref. [26], the integral subtraction on the left-hand side relates to a quadratic divergence in the VPE. By this subtraction we restore gauge invariance, which is not manifest for the Jost function. Note that we can write that integral as

$$n^2 \int_{\rho_{\min}}^{\infty} \frac{d\rho}{\rho} g^2(\rho) = \sum_{\ell} \int_{\rho_{\min}}^{\infty} \frac{d\rho}{\rho} J_\ell^2(qr) [n^2 g^2(\rho) - 2n\ell g(\rho)],$$

where the $J_\ell(z)$ are cylindrical Bessel functions. This integral then replaces the leading Born approximation from the singular terms in the wave-equation. Its contribution to $\nu_\ell(t)$ arises from an integration by parts of an expression that contains its derivative with respect to t , *cf.* Eq. (48). Hence subtracting a constant times this quantity has no effect on the result, but renders the integral well-defined on the imaginary axis.

In $D = 3 + 1$, the right-hand side of Eq. (63) still contains a logarithmic divergence, which we computed in dimensional regularization. It actually arises from a combination of two Feynman diagrams that individually are quadratically divergent, *cf.* Eq. (25). The analogous Born expansions would have to be performed individually. However, for the singular vortex configuration, these integrals do not exist. Hence we apply the fake boson formalism developed in Ref. [27] as described above. As shown in Eq. (45), the second-order term for a scalar field also yields a logarithmic divergence. In principle, the strength of that divergence does not depend on the mass of the boson. We take it to equal the classical Higgs/gauge mass so that we can simply subtract the associated Born term from $\nu_\ell(t)$ with a suitably adjusted strength and add it back as a Feynman diagram. To be precise, we consider scattering of a boson in the potential $V_f(\rho) = 3(\tanh^2(\kappa\rho) - 1)$, for which $\bar{\nu}_\ell^{(2)}(t)$ is the second-order contribution to the Jost function on the imaginary momentum axis. The partial wave expansion for this scalar field is similar to that of ghost field in Eq. (19) with $2(h(\rho) - 1)$ replaced by $V_f(\rho)$. We take κ as an arbitrary parameter to later test our numerical simulation, since the final result for VPE should not depend on a particular choice for V_f . This subtraction is calibrated by Eq. (44), which for this particular scalar potential reads

$$c_B = -\frac{e^2 \int_0^\infty r dr F_{\mu\nu} F^{\mu\nu}}{6 \int_0^\infty r dr V_f^2} = -\frac{n^2 \int_0^\infty \rho d\rho \left(\frac{g'(\rho)}{\rho} \right)^2}{3 \int_0^\infty \rho d\rho [3(\tanh^2(\kappa\rho) - 1)]^2}. \quad (64)$$

C. VPE for $D = 2 + 1$ and $D = 3 + 1$

As mentioned above, our analysis proceeds with dimensionless variables such that $ev = 1$. We return to dimensionful expressions by multiplying with appropriate powers of $\frac{M}{\sqrt{2}}$ where M is the Higgs mass, which does not acquire quantum correction in our on-shell scheme.

For $D = 3 + 1$, the ghost and non-transverse gauge field contributions cancel. In that case, however, we still have to integrate over the momentum conjugate to the symmetry axis using the interface formalism of Eq. (53). For later

discussion we separate the scattering contribution (including the factor of two for the complex fields) after the fake boson subtraction,

$$\Delta E_{\text{scat.}} = \frac{M^2}{2} \int_{\sqrt{2}}^{\infty} \frac{dt}{2\pi} t \{[\nu(t)]_V - c_B \nu_B(t)\}. \quad (65)$$

Here $\nu_B(t)$ is the angular momentum sum of the second Born contribution to the logarithm of the Jost function from the fake boson potential.

To evaluate the renormalized Feynman diagram contributions, we introduce Fourier transforms of the vortex profiles

$$\begin{aligned} I_A(q) &= n \int_0^{\infty} d\rho h(\rho) g(\rho) J_1(q\rho), & I_H(q) &= q \int_0^{\infty} \rho d\rho [1 - h(\rho)] J_0(q\rho), \\ \tilde{v}_H(q) &= \int_0^{\infty} \rho d\rho [h^2(\rho) - 1] J_0(q\rho), & \tilde{v}_f(q) &= 3 \int_0^{\infty} \rho d\rho [\tanh^2(\kappa\rho) - 1] J_0(q\rho), \end{aligned} \quad (66)$$

where, again, the $J_\ell(z)$ are cylindrical Bessel functions.

In $D = 3 + 1$ we have logarithmic divergences at second order, and we therefore separate the finite counterterm

$$E_{\text{CT}} = \frac{M^2}{16\pi} \int_0^{\infty} \rho d\rho \left\{ \left[17 - 10 \frac{\pi}{\sqrt{3}} \right] \left[h'^2 + n^2 \frac{h^2}{\rho^2} g^2 \right] + \frac{1}{2} \left[35 - 19 \frac{\pi}{\sqrt{3}} \right] [h^2 - 1]^2 + \frac{c_B}{18} \left[22 - 5\sqrt{3}\pi \right] \left(\frac{ng'}{\rho} \right)^2 \right\}. \quad (67)$$

and the finite Feynman diagram contributions

$$E_{\text{FD}} = \frac{M^2}{2\pi} \int_0^{\infty} dq \left[I_A^2(q) + I_H^2(q) + \frac{13}{8} \tilde{v}_H^2(q) + \frac{c_B}{8} \tilde{v}_f^2(q) \right] \left[\sqrt{q^2 + 8} \operatorname{asinh} \left(\frac{q}{\sqrt{8}} \right) - q \right]. \quad (68)$$

Recall that $\tilde{v}_f(q)$ was defined after Eq. (45).

In $D = 2 + 1$, the second order contributions do not lead to an ultra-violet divergence. Nevertheless it is convenient to subtract them from the scattering data and add them back as Feynman diagrams, because it allows us to use the same $[\nu(t)]_V$ as above. We separate the scattering contribution in Eq. (51) and augment it by the ghost piece

$$\Delta E_{\text{scat.}} = \frac{M}{\sqrt{2}} \left\{ \int_{\sqrt{2}}^{\infty} \frac{dt}{\pi} \frac{t}{\sqrt{t^2 - 2}} \{[\nu(t)]_V - c_B \nu_B(t)\} - \int_{\sqrt{2}}^{\infty} \frac{dt}{2\pi} \frac{t}{\sqrt{t^2 - 2}} \nu_{\text{gh}}(t) \right\}, \quad (69)$$

where $\nu_{\text{gh}}(t)$ is the angular momentum sum of the logarithm of the Jost function with two Born subtractions for the single channel potential $V_{\text{gh}} = 2(\Phi_S^2 - v^2) = 2v^2(h^2(\rho) - 1)$. In comparison with Eq. (51), a factor of two again appears in the first integral because we are dealing with a complex boson field. Note that this first integral in Eq. (69) would also be finite without the fake boson subtraction. However, its inclusion improves the large momentum convergence of that integral and is thus advantageous in the numerical simulation.

The final ingredient is the renormalized Feynman diagram contribution in $D = 2 + 1$,

$$\begin{aligned} E_{\text{FD}} &= -\sqrt{2}M \int_0^{\infty} dq \left[I_A^2(q) + I_H^2(q) + \frac{11}{8} \tilde{v}_H^2(q) + \frac{c_B}{8} \tilde{v}_f^2(q) \right] \arctan \left(\frac{q}{\sqrt{8}} \right) \\ E_{\text{CT}} &= \frac{M}{48} \int_0^{\infty} \rho d\rho \left\{ [45 \ln(3) - 28] \left[h'^2 + n^2 \frac{h^2}{\rho^2} g^2 \right] + \frac{1}{2} [87 \ln(3) - 28] [h^2 - 1]^2 + \frac{1}{2} [3 \ln(3) + 4] \left(\frac{ng'}{\rho} \right)^2 \right\}. \end{aligned} \quad (70)$$

As in Eq. (68), factors of $1/\sqrt{2}$ emerged in the arguments of the trigonometric and hyperbolic functions in the counterterm contribution because $M = \sqrt{2}ev$.

VI. NUMERICAL RESULTS FOR THE VPE

As a first step we substitute the profile functions with the parameterization of Eq. (9) into \mathcal{V} and $\bar{\mathcal{V}}$ in Eqs. (57) and (59), respectively. For a given angular momentum channel, we then integrate the differential equations (55) and (60) with the appropriate boundary conditions from a large $\rho_{\text{max}} \approx 20$ to a small ρ_{min} near the center of the vortex. Once ρ_{min} is small enough, we compute

$$\nu_L(t) = \sum_{\ell=-L}^L \left[\nu_\ell(t) - \bar{\nu}_\ell^{(1)}(t) - \bar{\nu}_\ell^{(2)}(t) \right]_{\rho_{\text{min}}} - n^2 \int_{\rho_{\text{min}}}^{\infty} \frac{d\rho}{\rho} g^2(\rho). \quad (71)$$

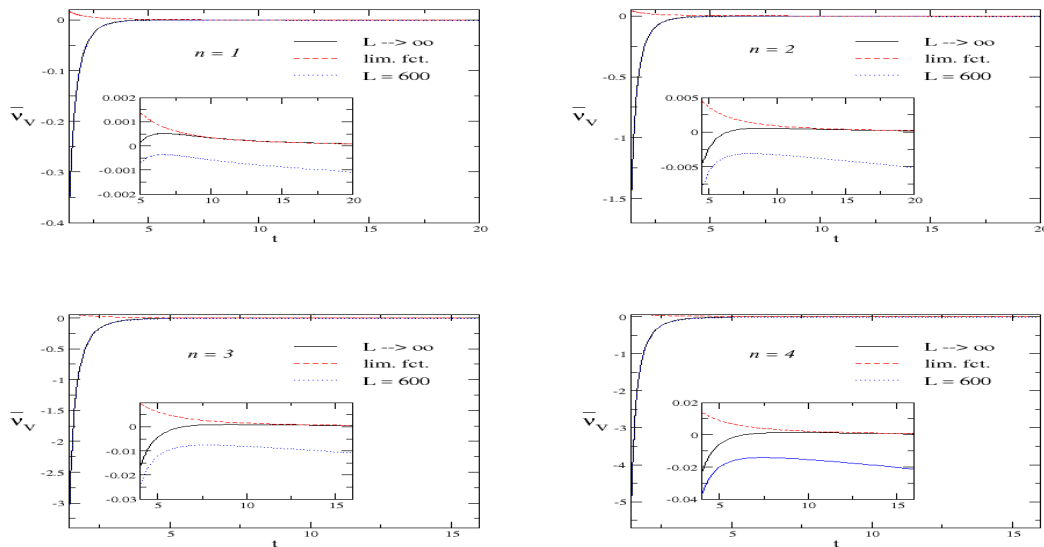


FIG. 2: Large angular momentum extrapolation from Eq. (71). The line labeled *lim. fct.* refers to the large t behavior in Eq. (63).

We find that there are still small variations when decreasing ρ_{\min} even further. These variations emerge from channels that do not have an angular momentum barrier at the center of the vortex. In those instances, the regular and irregular solutions respectively approach a constant and logarithm, which are difficult to disentangle numerically. According to Eq. (18) these are the $\ell = -1$ and $\ell = n$ channels. In those channels we use several small values for ρ_{\min} and fit

$$\ln \det \mathcal{F}_\ell - \overline{\mathcal{F}}_\ell^{(1)} - \overline{\mathcal{F}}_\ell^{(2)} - \frac{1}{2} \left(\overline{\mathcal{F}}_\ell^{(1)} \right)^2 = a_0 + \frac{a_1}{\ln(\rho_{\min})} + \frac{a_2}{\ln^2(\rho_{\min})}$$

and replace the square bracket in Eq. (71) by a_0 for these ℓ -values. We note that this fit is also needed for regular gauge profiles even though they have well-defined Born series, because there one still has to disentangle constant and logarithm behaviors [28]. We remark that the cancellations of the ρ_{\min} singularities in Eq. (71) stems from the large L terms in that sum.

It is essential to verify that $[\nu(t)]_V$ exhibits the asymptotic behavior predicted in Eq. (63) by the analysis of the two-point function for the gauge field. It turns out that even summing up to a large value like $L = 600$ is insufficient to compute the sum on the left-hand side. As explained in Ref. [26], on top of computing the sum for such large values of L , an extrapolation for $L \rightarrow \infty$ is needed. This is done by using different large values of L in Eq. (71) and extracting $[\nu(t)]_V$ from a fit of the form $\nu_L(t) \approx [\nu(t)]_V + \frac{b_1}{L} + \frac{b_2}{L^2}$. The importance of this extrapolation is shown in the inserts of Fig. 2. Though the numerical effect appears to be small, we note that the integrand for $D = 3 + 1$ in Eq. (65) has an additional factor of t , which amplifies any inaccuracy at large t . Also, without that extrapolation the integrand may incorrectly appear to converge without subtractions already at moderate t [26], which has led to incorrect conclusions in the past [15].

As suggested by this discussion, the numerical simulation is quite costly in computation time.³ We therefore compute $[\nu(t)]_V$ for about 200 different t values and implement a Laguerre interpolation to obtain a smooth function. This interpolation also allows for the substitution to $\tau = \sqrt{t^2 - 2}$, which avoids the integrable singularity in Eq. (69). The final VPE is simply the sum

$$\Delta E = E_{\text{FD}} + E_{\text{CT}} + \Delta E_{\text{scat.}} \quad (72)$$

In Table II we present our results for the VPE of the vortex for $D = 2 + 1$. We also list the Feynman diagram and counterterm contributions from Eq. (70) as well as the scattering piece from Eq. (69) with the extrapolations

³ For large angular momenta sufficient accuracy can only be accomplished with *long-double* precision. This adds considerably to the computation time.

described above. While the cancellations between the Feynman diagram and counterterm pieces are expected, the fact that their combination goes in the same direction as the scattering piece is somewhat surprising. Overall, we find that the total VPE is always negative.

	$n = 1$	$n = 2$	$n = 3$	$n = 4$
E_{CT}	0.2671	0.4819	0.6786	0.8662
E_{FD}	-0.5156	-1.1365	-1.7588	-2.3877
$\Delta E_{\text{scat.}}$	-0.2484	-0.6546	-1.0801	-1.5215
ΔE	-0.0882	-0.3408	-0.6631	-1.0205
	-0.3367	-0.9955	-1.7432	-2.5420

TABLE II: Various contributions to the VPE of BPS vortices for $D = 2 + 1$. E_{CT} and E_{FD} are the sums of all listed counterterm contributions, including the fake boson. All data are in units of $M = \sqrt{2}ev$.

	$n = 1$	$n = 2$	$n = 3$	$n = 4$
E_{CT}	-0.0134	-0.0212	-0.0272	-0.0325
E_{FD}	0.0212	0.0157	0.0158	0.0167
$\Delta E_{\text{scat.}}$	0.0078	-0.0054	-0.0114	-0.0157
ΔE	-0.0255	-0.0969	-0.1782	-0.2622
	-0.0177	-0.1023	-0.1896	-0.2784

TABLE III: Various contributions to the VPE of BPS vortices for $D = 3 + 1$. Scattering data as before, E_{CT} and E_{FD} are the sums of all listed counterterm contributions, including the fake boson. All data are in units of $M^2 = 2(ev)^2$.

Table III contains our results for the VPE per unit length of the vortex in $D = 3 + 1$. The ingredients for Eq. (72) are taken from Eqs. (65), (67) and (68). Somewhat unexpectedly, the counterterm and Feynman diagram contributions go in the same direction, presumably because E_{CT} involves timelike momenta while E_{FD} is an integral over spacelike momenta. On the other hand there is a substantial cancellation between the scattering and Feynman diagram contributions once they are combined with the counterterms that implement the on-shell renormalization. In both $D = 2 + 1$ and $D = 3 + 1$, $\Delta E_{\text{scat.}}$ is sizable, which is a clear indication that the VPE cannot be reliably computed from only low order Feynman diagrams.

In $D = 3 + 1$ the VPE is essentially linear in the winding number n . We fit the data from Table III as: $\Delta E = -0.0166 - 0.0869(n - 1)$. The quality of the fit is measured as $\chi^2 = 4.4 \times 10^{-6}$. To obtain a similarly small $\chi^2 = 7.2 \times 10^{-5}$ in $D = 2 + 1$ we need to add a quadratic contribution $\Delta E = -0.3348 - 0.6314(n - 1) - 0.0350(n - 1)^2$, but the coefficient of that contribution is quite small.

We observe qualitatively similar winding number dependences in $D = 2 + 1$ and $D = 3 + 1$. An analogous similarity between these two cases was also found for the fermion VPE of QED flux tubes once equivalent renormalization conditions were implemented [29].

We have already performed a consistency test of our results when comparing the large momentum behavior of \bar{v}_V in Figure 2. We have also verified the independence with respect to the fake boson potential $V_f(\rho)$ by using different values for the mass parameter κ . We show an example in Table IV with two κ values for $n = 4$ for both $D = 2 + 1$ and $D = 3 + 1$. The entries for $\kappa = 0.7$ are those from Tables II and III. The variation with κ of the individual components is small but significant, and when combined to ΔE these variations indeed cancel.

	$\kappa = 0.7$	$\kappa = 1.0$		$\kappa = 0.7$	$\kappa = 1.0$
$\Delta E_{\text{scat.}}$	-1.02049	-1.01919	$\Delta E_{\text{scat.}}$	-0.26264	-0.26219
$E_{\text{FD}} + E_{\text{CT}}$	-1.52148	-1.52278	$E_{\text{FD}} + E_{\text{CT}}$	-0.01574	-0.01620
ΔE	-2.54197	-2.54197	ΔE	-0.27839	-0.27839

TABLE IV: Dependence of components of the VPE on the fake boson parameter κ for $n = 4$. Left panel: $D = 2 + 1$, right panel: $D = 3 + 1$.

Our results for the scattering data contributions $\Delta E_{\text{scat.}}$ generally agree with those of Ref. [14], in particular on the sign and the tendency with increasing winding number n . Those authors employed a truncated heat kernel expansion with ζ -function regularization. This amounts to an $\overline{\text{MS}}$ renormalization scheme and we have thus compared their results to $\Delta E_{\text{scat.}}$. We do not agree with the sign in the prediction presented⁴ in Ref. [13] for $n = 1$ and $D = 3 + 1$.

⁴ The erratum to Ref. [13] has a sign change compared to the original publication.

As in that study we reproduce the significant cancellation between scattering and Feynman diagram contributions. Ref. [13] constructs a local density of states using the Green's function at coincident points, which in turn relies on scattering data along the imaginary momentum axis; this approach is essentially equivalent to ours, because the integral over space of the Green's function yields the Jost function that we compute. Apart from the different sign we also find that our results are smaller in magnitude. This may be due to the angular momentum extrapolation, since as we have seen the extrapolation from $L \approx 35$ they use is likely insufficient [26]. In addition, the Green's function approach requires an additional integral over the radial coordinate, which may be a source of numerical inaccuracies. As a final source of the disagreement, we note that Ref. [13] imposes the $\overline{\text{MS}}$ renormalization scheme at the scale of the un-renormalized gauge boson mass. In an earlier proof of concept investigation of the $D = 3 + 1$ case we used a simplified on-shell scheme [10]. Comparison reveals that different schemes can easily change the sign of the small $n = 1$ VPE. However, they do not alter the (almost) linear dependence on the winding number.

VII. CONCLUSIONS

We have computed the one-loop quantum corrections to the energy (per unit length) of ANO vortices in scalar electrodynamics with spontaneous symmetry breaking, in the BPS case where the classical masses of the scalar and gauge fields are equal. These corrections arise from the polarization of the spectrum of quantum fluctuations in the classical vortex background. This vacuum polarization energy is small because the small coupling approximation applies to electrodynamics with $e^2 = 4\pi/137 \approx 0.09$, but it becomes decisive in the case of observables for which the classical result vanishes, such as the binding energies of vortices with higher winding numbers in the BPS case.

After clarifying a number of technical and numerical subtleties, we found that the dominant contribution to vacuum polarization energies of vortices stems from the non-perturbative contribution, which cannot be computed from the lowest order Feynman diagrams; these diagrams represent an expansion in the background fields rather than the coupling constant. Our numerical simulations for vortices with winding number up to four suggest that the quantum energy weakly binds higher winding number BPS vortices. We have also seen that the vacuum polarization energy for the unit winding number vortex is very small, so that at first glance it appears to be compatible with zero up to numerical errors. The potentially most important source for such errors is the small radius behavior in channels that contain zero angular momentum components. However, our numerical analysis suggests that any improvement of the data is small and likely to push that vacuum polarization energy further away from zero.

To our knowledge these are the first studies of a static soliton vacuum polarization energy that compare different topological sectors in a renormalizable model. The vortex model has two nontrivial space dimensions. Solitons in one space dimension do either not have topologically distinct⁵ static solitons, such as the kink and sine-Gordon soliton [30], or are destabilized by the quantum corrections, such as the ϕ^6 model soliton [31]. The Skyrme model [32] in three space dimensions indeed has static solitons with different winding numbers, but unfortunately that model is not renormalizable.

For $D = 2 + 1$ and $D = 3 + 1$ the VPE (approximately) decreases linearly with the winding number n with some offset at $n = 0$. For the binding energies $\Delta E - n\Delta E|_{n=1}$ we get $-0.297(n - 1) - 0.035(n - 1)^2$ and $-0.070(n - 1)$, respectively. Since in the BPS case the classical binding energy is strictly zero, this implies that it is energetically favorable for vortices to coalesce rather than to appear in isolation. This observation is characteristic of a type I superconductor. We also observe that $\Delta E|_{n=4} - 2\Delta E|_{n=2} < 0$ and $\Delta E|_{n=3} - \Delta E|_{n=2} - \Delta E|_{n=1} < 0$, making the existence of substructures unlikely.

Away from the BPS case, the classical binding energy can quickly overwhelm the quantum correction since the model is weakly coupled. Nevertheless, the computation of vacuum polarization energies for unequal masses would be desirable to complete this picture. Technically this calculation is more involved because it corresponds to a full 4×4 scattering problem, rather than a doubled 2×2 problem. Another interesting question is whether the techniques to avoid divergences in the Fourier transform of the vortices that was developed in Ref. [26] and employed here will also be successful when coupling fermions and thus avoid the necessity of a *return flux* [29]. If this is the case, supersymmetric extensions [33] can be investigated as well. We also conjecture that analogous calculations are possible in the case of a 't Hooft-Polyakov monopole [34, 35].

⁵ There are different topological sectors in these models but the corresponding solitons solutions are constructed from those with the lowest nonzero winding number. For example, the $n = 2$ sine-Gordon solution is the superposition of two (infinitely) widely separated $n = 1$ solutions.

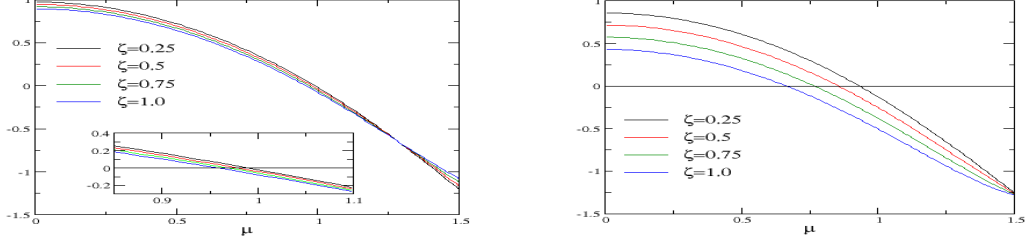


FIG. 3: Right-hand sides for the implicit Eqs. (A2). Left panel: $D = 2 + 1$, right panel: $D = 3 + 1$.

μ	$n = 1$	$n = 2$	$n = 3$	$n = 4$
0.92	0.0017	0.0028	0.0048	0.0069
0.94	0.0008	0.0021	0.0036	0.0053
0.96	0.0006	0.0015	0.0025	0.0036
0.98	0.0003	0.0007	0.0013	0.0018

TABLE V: Gauge mass variation of the VPE, E_μ , for $D = 2 + 1$ in units of M according to Eq. (A1).

Acknowledgments

N. G. is supported in part by the National Science Foundation (NSF) through grants PHY-1820700 and PHY-2205708. H. W. is supported in part by the National Research Foundation of South Africa (NRF) by grant 109497.

Appendix A: Higher order effects from the wave-function renormalization of the gauge field

In this Appendix we briefly discuss the higher order effects of $\mu \neq 1$. These arise via the wave-function counterterm for the gauge field in Eq. (24). The changes in the energies are

$$\begin{aligned}
 E_\mu &= -\frac{M}{96} \left[\frac{12}{4 - \mu^2} + \frac{6}{\mu} \operatorname{atanh} \left(\frac{\mu}{2} \right) - 4 - 3 \ln(3) \right] \int_0^\infty \rho d\rho \left(n \frac{g'}{\rho} \right)^2, \\
 E_\mu &= \frac{M^2}{288\pi} \left[\frac{24}{\mu^2} (1 - \mu^2) + 5\sqrt{3}\pi - \frac{6}{\mu^3} \frac{\mu^4 - 2\mu^2 + 16}{\sqrt{4 - \mu^2}} \operatorname{asin} \left(\frac{\mu}{2} \right) \right] \int_0^\infty \rho d\rho \left(n \frac{g'}{\rho} \right)^2
 \end{aligned} \tag{A1}$$

for $D = 2+1$ and $D = 3+1$, respectively. These changes are the differences of the gauge field counterterm contributions evaluated at μ and $\mu = 1$. Interestingly, we do not need to explicitly solve Eqs. (41) and (42) to determine μ for given values of e and M , as long as we measure the energies in units of M and M^2 . However, before we compute E_μ , we must identify the range of solutions to these equations. We therefore write them as

$$\begin{aligned}
 0 &= 1 - \mu^2 + \zeta \left[\frac{15}{8} \ln(3) - \frac{13}{6} + \frac{\mu^2}{2(4 - \mu^2)} - \frac{\mu}{4} \operatorname{atanh} \left(\frac{\mu}{2} \right) \right] \\
 0 &= 1 - \mu^2 + \zeta \left[\frac{9}{2} - \frac{5\pi}{\sqrt{3}} - \frac{\mu^2}{6} + \frac{16 - 2\mu^2}{\mu\sqrt{4 - \mu^2}} \operatorname{asin} \left(\frac{\mu}{2} \right) \right],
 \end{aligned} \tag{A2}$$

with the dimensionless parameters $\zeta = \frac{e^2}{2\pi M}$ and $\zeta = \frac{e^2}{8\pi^2}$ for $D = 2+1$ and $D = 3+1$, respectively. The singularity at $\mu = 2$ emerges from virtual Higgs particles going on-shell and allowing the gauge particle to decay into two Higgses. Even if this singularity produces a zero crossing Eq. (A2), we consider it unphysical because it does not smoothly emerge from the tree-level result. Such a solution would approach $\mu = 2$ as $\zeta \rightarrow 0$.

We display the right-hand sides of Eq. (A2) in Figure 3. For $D = 2 + 1$, only a narrow window below $\mu = 1$ is accessible even for un-realistically large values of ζ . On the other hand, for $D = 3 + 1$ it seems acceptable to have $\mu \in [0.8, 1]$. In Tables V and VI we present the numerical results for E_μ in the appropriate ranges of μ . Compared

μ	$n = 1$	$n = 2$	$n = 3$	$n = 4$
0.80	0.0004	0.0011	0.0018	0.0027
0.85	0.0003	0.0009	0.0014	0.0021
0.90	0.0002	0.0006	0.0010	0.0015
0.95	0.0001	0.0003	0.0005	0.0008

TABLE VI: Gauge mass variation of the VPE, E_μ , for $D = 3 + 1$ in units of M^2 according to Eq. (A1).

to the data in Tables II and III, these contributions are tiny and do not effect our conclusions on the VPE.

-
- [1] A. A. Abrikosov, Sov. Phys. JETP **5**, 1174 (1957).
[2] A. A. Abrikosov, Journal of Physics and Chemistry of Solids **2**, 199 (1957).
[3] H. B. Nielsen and P. Olesen, Nucl. Phys. B **61**, 45 (1973).
[4] M. Tinkham, *Introduction to Superconductivity* (Dover, Mineola, New York, 1996).
[5] Y. Nambu, Nucl. Phys. B **130**, 505 (1977).
[6] T. W. B. Kibble, J. Phys. A **9**, 1387 (1976).
[7] E. P. S. Shellard and A. Vilenkin, *Cosmic Strings and Other Topological Defects* (Cambridge University Press, Cambridge, UK, 1994).
[8] E. B. Bogomolny, Sov. J. Nucl. Phys. **24**, 449 (1976).
[9] M. K. Prasad and C. M. Sommerfield, Phys. Rev. Lett. **35**, 760 (1975).
[10] N. Graham and H. Weigel, Int. J. Mod. Phys. A **37**, 2241004 (2022).
[11] N. Graham, M. Quandt, and H. Weigel, *Spectral Methods in Quantum Field Theory*, vol. 777 (Springer-Verlag, Berlin, 2009).
[12] N. Graham and H. Weigel, Phys. Rev. **D104**, L011901 (2021).
[13] J. Baacke and N. Kevlishvili, Phys. Rev. **D78**, 085008 (2008), [Erratum: Phys. Rev. D **82**, 129905 (2010)].
[14] A. Alonso-Izquierdo, J. Mateos Guilarte, and M. de la Torre Mayado, Phys. Rev. D **94**, 045008 (2016).
[15] P. Pasipoularides, Phys. Rev. **D64**, 105011 (2001).
[16] N. Graham, R. L. Jaffe, M. Quandt, and H. Weigel, Phys. Rev. Lett. **87**, 131601 (2001).
[17] A. Rebhan, P. van Nieuwenhuizen, and R. Wimmer, Braz. J. Phys. **34**, 1273 (2004).
[18] B.-H. Lee and H. Min, Phys. Rev. D **51**, 4458 (1995).
[19] C. Becchi, A. Rouet, and R. Stora, Commun. Math. Phys. **42**, 127 (1975).
[20] N. Irges and F. Koutroulis, Nucl. Phys. B **924**, 178 (2017), [Erratum: Nucl.Phys. B **938**, 957–960 (2019)].
[21] J. S. Faulkner, J. Phys. **C10**, 4661 (1977).
[22] F. Calegero, *Variable Phase Approach to Potential Scattering* (Academic Press, New York, 1967).
[23] R. G. Newton, *Scattering Theory of Waves and Particles* (Springer, New York, 1982).
[24] M. Bordag and K. Kirsten, Phys. Rev. **D53**, 5753 (1996).
[25] N. Graham, R. L. Jaffe, M. Quandt, and H. Weigel, Annals Phys. **293**, 240 (2001).
[26] N. Graham and H. Weigel, Phys. Rev. **D101**, 076006 (2020).
[27] E. Farhi, N. Graham, R. L. Jaffe, and H. Weigel, Nucl. Phys. B **630**, 241 (2002).
[28] N. Graham, M. Quandt, and H. Weigel, Phys. Rev. D **84**, 025017 (2011).
[29] N. Graham, V. Khemani, M. Quandt, O. Schröder, and H. Weigel, Nucl. Phys. B **707**, 233 (2005).
[30] R. Rajaraman, *Solitons and Instantons* (North Holland, Amsterdam, 1982).
[31] H. Weigel, AIP Conf. Proc. **2116**, 170002 (2019).
[32] T. H. R. Skyrme, Proc. Roy. Soc. Lond. A **260**, 127 (1961).
[33] J. D. Edelstein, C. Nunez, and F. Schaposnik, Phys. Lett. B **329**, 39 (1994).
[34] G. 't Hooft, Nucl. Phys. B **79**, 276 (1974).
[35] A. M. Polyakov, JETP Lett. **20**, 194 (1974).